

FEATURE ARTICLE

Modeling the Interactions between Polymer-Coated Surfaces

Chandralekha Singh, Galen T. Pickett, Ekaterina Zhulina, and Anna C. Balazs*

Chemical and Petroleum Engineering Department, University of Pittsburgh, Pittsburgh, Pennsylvania 15261

Received: August 1, 1997; In Final Form: October 6, 1997[⊗]

Using a two-dimensional self-consistent field calculation and scaling theory, we investigate the interaction between two planar surfaces where: (1) each surface is grafted with both solvophilic *and* solvophobic homopolymers and (2) both surfaces are coated with solvophobic polyelectrolytes. The chains are tethered by one end and grafted at relatively low densities. For both systems, we determine the morphology of the layers and the energy of interaction as the layers are compressed. The energy of interaction versus distance profiles show a wide region of attraction as the surfaces are brought together. This attractive interaction is due to the self-assembled structures that appear at low grafting densities in poor solvents. Furthermore, for polyelectrolytes at high degrees of ionization (α), compressing the layers results in a novel first-order phase transition: the uniformly stretched, charged chains spontaneously associate into aggregates (pinned micelles) on the surfaces. At both low and high α , the free energy versus distance profiles reveal distinct minima, which indicate an optimal separation between the surfaces. Our findings provide guidelines for controlling the interactions between coated colloidal particles and yield design criteria for driving colloids to self-assemble into ordered arrays.

Introduction

The interactions between solid surfaces can be controlled by attaching polymer chains to these interfaces. For example, polymer coatings on pigments and other colloids are responsible for keeping these particles suspended in solution.¹ Here, the anchored polymers form a thick corona around the particle. The repulsion between coronas on neighboring particles prevents the colloids from aggregating and thereby stabilizes the suspension. Such polymer coatings also play a critical role in reducing the friction between mechanical components. As these components come into contact, the polymer layer acts as a lubricant, decreasing the wear between the parts and increasing the lifetime of the machinery.

The polymers are commonly attached to the surface by one end of the chain and thus are referred to as “terminally-anchored” or “end-grafted”. The attachment can be accomplished by placing a surface-active group on the end of the polymer or growing the chains with monomers in solution at reactive “seed” or initiator sites on the surface. The interaction between the polymer-coated surfaces are determined by the conformation of these anchored chains. For end-grafted polymers immersed in a compatible (good) solvent, the conformation of the chains is relatively well characterized.² In particular, the well-solvated (or solvophilic) chains extend into the solution and form a spatially uniform layer. The height of this layer, H , scales with N , the degree of polymerization of the chains. Compressing two homopolymer-coated surfaces in a good solvent gives rise to a repulsive interaction between the layers.³ The repulsion arises from the entropic losses that occur when the stretched, solvent-compatible chains are confined to the narrow region between the compressed substrates. This entropic repulsion is responsible for the polymeric stabilization of

colloidal particles noted above. These interfaces would also form effective lubricants, since the polymer layer acts as a barrier to contacts between the surfaces.

The structure of end-grafted chains in incompatible, or poor, solvents is quite different from that in good solvents. At relatively high grafting densities, the tethered chains avoid the poor solvent by shrinking into a thin, uniform layer.⁴ On the other hand, when the chains are grafted at relatively low densities, the system exhibits particularly dramatic behavior. Here, the solvophobic polymers escape the unfavorable solution by clustering with neighboring chains into distinct aggregates, or “pinned micelles”.^{5,6} (These structures are “pinned” since the ends of the chains are immobilized on the surface.) Recent experimental observations⁷ have confirmed theoretical predictions^{5,6} concerning the existence of these pinned micelles. When two surfaces that are covered with pinned micelles are brought into close contact, the solvophobic interactions drive the micelles from the opposite surfaces to merge and form a larger aggregate between the substrates.⁸ In this way, more of the tethered chains are effectively shielded from the unfavorable solvent and the free energy of the system is lowered. Consequently, the surfaces undergo a net attraction, and these layers can act as effective adhesives between the substrates.

Little, however, is known about the interactions between polymer-coated surfaces when we move away from these simple cases of tethered *homopolymers* in good or poor solvents. For example, there have been few studies on the interactions between surfaces that are coated with both solvophilic (A) *and* solvophobic (B) homopolymers,^{9–11} or are coated with copolymers that contain multiple reactive blocks.^{12,13} The goal of our research has been to investigate these more complex systems through theoretical models that reveal the morphology of the layers between the substrates and allow us to calculate the interaction energies between the surfaces.^{10–14} Using these models, we demonstrate that tethering *both* A and B homopoly-

* To whom correspondence should be addressed.

⊗ Abstract published in *Advance ACS Abstracts*, November 15, 1997.

mers on *each* of the substrates provides a handle for engineering the interactions between the surfaces.¹⁰ In particular, by varying the relative length and grafting density of the different chains, we can achieve a high degree of control over the surface interactions and tailor these interactions for the desired applications.

Another way of enriching the phase behavior and increasing the utility of these systems is to tether charged polymers, or polyelectrolytes, on the surface. Below, we show that the structure of the anchored polyelectrolyte layer can be abruptly altered by compressing the two surfaces within a poor solvent.¹⁴ This structural transformation drives the surfaces into closer contact, despite an overall electrostatic repulsion. These findings yield new guidelines for driving colloidal particles to self-assemble into ordered arrays.

In addition to providing design criteria for modifying surface interactions, our results illustrate the striking effect that confining polymer layers between two surfaces can have on the morphology of the system. In effect, it is these morphological changes that we exploit to tailor the macroscopic behavior of the system. We begin our discussion by providing a brief description of our theoretical models, two-dimensional self-consistent field calculations and scaling theory, and then describe our results on compressing polymer-coated surfaces.

The Models

The self-consistent field (SCF) calculations provide a description of the system at thermodynamic equilibrium. One-dimensional SCF theory, however, is insufficient for describing the structure of laterally inhomogeneous structures such as pinned micelles. We therefore use a two-dimensional SCF theory,^{8,10–16} which is a generalization of the 1D model developed by Scheutjens and Fleer.¹⁷ In the Scheutjens and Fleer theory, the phase behavior of polymer systems is modeled by combining Markov chain statistics with a mean field approximation. Since the method is thoroughly described in ref 17, we simply provide the basic equations and refer the reader to that text for a more detailed discussion.

Here, we limit our comments to the behavior of linear polymers. These calculations involve a planar lattice where one lattice spacing represents the length of a statistical segment within a polymer chain. The planar lattice is divided into $z = 1$ to M layers. In the one-dimensional model, the properties of the system only depend on z , the direction perpendicular to the interface. The properties of the system are averaged over the x and y directions; that is, the system is assumed to be translationally invariant in the lateral direction. The probability that a monomer of type i is in layer z with respect to the bulk is given by the factor

$$G_i(z) = \exp(-u_i(z)/kT) \quad (1)$$

where the potential $u_i(z)$ for a segment of type i in layer z is given by

$$u_i(z) = u'(z) + kT \sum_{j(\neq i)} \chi_{ij} (\langle \phi_j(z) \rangle - \phi_j^b) \quad (2)$$

The parameter $u'(z)$ is a “hard-core potential”, which ensures that every lattice layer is filled. In the second term, χ_{ij} is the Flory–Huggins interaction energy between units i and j and ϕ_j^b is the polymer concentration in the bulk. The expression $\langle \phi_j(z) \rangle$ is the fraction of contacts an i segment in the z layer makes with j -type segments in the adjacent layers and is given by the following equation:

$$\langle \phi_j(z) \rangle = \lambda_{-1} \phi_j(z-1) + \lambda_0 \phi_j(z) + \lambda_1 \phi_j(z+1) \quad (3)$$

Here, the λ 's are the fraction of neighbors in the adjacent layers: λ_{-1} is for the previous layer, λ_0 is for the same layer, and λ_1 is for the next layer.

Since polymers contain more than one segment, we must take into account that the segments of the chain are connected. We define $G_i(z,s|1)$ as the (conditional) probability (up to a normalization constant) that a segment s is located in layer z , while being connected to the first segment of chain i . This Green's function can be calculated from the following recurrence relation:

$$G_i(z,s|1) = G_i(z) \{ \lambda_{-1} G_i(z-1,s-1|1) + \lambda_0 G_i(z,s-1|1) + \lambda_1 G_i(z+1,s-1|1) \} \quad (4)$$

Clearly, $G_i(z,1|1) = G_i(z)$ and the terms for $s > 1$ can be calculated from this relationship and eq 4. In the same way, we can obtain a recurrence formula for $G_i(z,s|r)$, the probability that a segment s is in layer z , given it is connected to the last (r th) segment of the chain.

To obtain the volume fraction of i in the z layer due to segment s , in a chain of r segments, the product of two probability functions is needed: the probability of a chain starting at segment 1 and ending with segment s in layer z and that of a chain starting at segment r and also ending with segment s in layer z . This product must be divided by $G_i(z)$ in order to compensate for the double counting of the s th segment. Hence, the volume fraction is given by

$$\phi_i(z,s) = C_i G_i(z,s|1) G_i(z,s|r) / G_i(z) \quad (5)$$

Here, C_i is the normalization constant and is equal to $C_i = \theta_i / r_i \sum_z G_i(z,r|1)$, where $\theta_i = \sum_z \phi_i(z)$ is the total amount of polymer segments of type i in the system and $\sum_z G_i(z,r|1) / M$ is the average of the end segment distribution function for a chain of r_i segments. We can also express C_i in terms of ϕ_i^b , the volume fraction in the bulk solution, as $C_i = \phi_i^b / r_i$. The total volume fraction of $\phi_i(z)$ of molecules i in layer z can be obtained by summing over s :

$$\phi_i(z) = \sum_s \phi_i(z,s) \quad (6)$$

Expressions 1, and 5, and the condition that $\sum_i \phi_i(z) = 1$ for each layer form a set of coupled equations that are solved numerically and self-consistently. Given that the amount of polymer, θ_i , the length r_i , and χ_{ij} are specified, we can calculate the self-consistent polymer profile and the equilibrium bulk concentration. (For a given θ_i , ϕ_i^b is obtained by equating the two expressions for C_i .)

We note that the expression for the excess free energy in terms of the segment density distribution is given by

$$F(z) = \sum_i \phi_i(z) \ln G_i(z) + (1/2) \sum_{jk} \chi_{j,k} \int \eta(z-z') \phi_j(z) \phi_k(z') dz' \quad (7)$$

where $\eta(z-z')$ is the short-range interaction function, which may be replaced by a summation over nearest neighbors. Summing the above equation over all z yields the total free energy. For two grafted layers, the free energy of interaction, ΔF_{int} , as a function of surface separation, L , can be obtained by taking the difference between the total free energies when the layers are infinitely apart and when they are separated by a distance L .

In the two-dimensional SCF theory,^{15,16} the above equations are explicitly written in terms of z and y , the directions perpendicular and parallel to the grafted layer, respectively. We assume translational invariance along x .

Using the 2D SCF model, we consider two planar surfaces that lie parallel to each other in the xy plane and investigate the

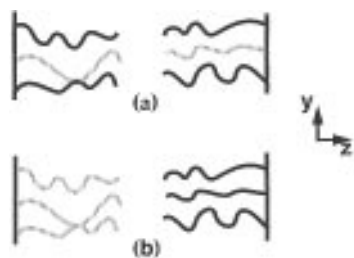


Figure 1. Schematic diagram of two end-grafted brushes: (a) with alternately grafted A–B chains and (b) with surfaces coated with homopolymers of different solvent qualities.

effect of bringing the surfaces closer together in the z direction. Each surface is covered with monodisperse end-grafted polymers. The ends of the chains are grafted to impenetrable surfaces at $z = 1$ and $z = L$. We apply periodic boundary conditions along the y direction.

The grafted polymers are characterized by three sets of parameters: grafting density, chain length, and the relevant χ parameters. The grafting density per line along the x direction is denoted by ρ and is fixed at $\rho = 0.025$ for all of the results presented below. (Thus, the average area per chain, s , has $s = 1/\rho$.) We emphasize that our calculations are restricted to the case of low grafting densities, where the formation of pinned micelles is most pronounced.^{5,6} As will be seen below, these structures have a dramatic influence on the interaction between the surfaces.

We let χ_{AS} and χ_{BS} represent the polymer–solvent interactions for the A and B components, respectively, and χ_{AB} is the interaction parameter for the two different monomers. The strength of interaction between the polymers and the planar, impenetrable surface is assumed to be the same as that between the polymer and the solvent. We fix the polymer–solvent interaction for the solvophilic A chains at $\chi_{AS} = 0$ and set $\chi_{BS} = 2$ for the solvophobic B chains. We also set $\chi_{AB} = 0$ and subsequently determine the effect of increasing $\chi_{AB} > 0$.

To complement our SCF calculations, we employ scaling theories. Through scaling theory, we formulate an expression for the free energy of our system. Minimizing this expression allows us to derive explicit relationships between the different variables in the system.^{10,13,14,18,19} The results of the scaling theory allow us to check and quantify the predictions from the SCF calculations. Conversely, we use the numerical calculations to verify various scaling predictions. How this scaling analysis is applied to the systems of interest is discussed in the relevant sections below.

Results and Discussion

Surfaces Grafted with A and B Homopolymers. We first discuss our findings from the SCF calculations for the case where A and B chains are grafted on each of the surfaces (see Figure 1a).¹⁰ Through this model, we can visualize the structural changes that occur within the grafted layer as the two polymer-coated surfaces are compressed. By calculating the appropriate free energies, we establish a qualitative relationship between the morphology of the layers and the surface interactions. To demonstrate the utility of grafting both types of chains on each of the substrates, we also describe the properties of a system where one surface is covered with just A chains and the other surface is coated with purely B polymers (see Figure 1b). Finally, we present a scaling model for the example of A and B chains on both surfaces.^{10,19} Through this model, we determine the explicit dependence of the surface interactions on the relative lengths and grafting densities of the tethered polymers.

The A and B homopolymers are grafted at alternate sites on each of the two surfaces,²⁰ as indicated in Figure 1a. As noted above, we fix $\chi_{AS} = 0$, $\chi_{BS} = 2$, and initially set $\chi_{AB} = 0$; the length of each chain is $N = 80$. Figure 2 shows how the self-assembly of the polymers is affected by the compression of the layers. At large surface separations (Figure 2a), the solvophobic B chains associate into pinned micelles and the A chains form an outer shell that encircles these regions. In this configuration, the B domains are shielded from the unfavorable solvent and the surface tensions within the system are minimized. Since the A chains are in a good solvent, they extend into the solution and their density slowly decays away from the B core. In effect, these aggregates have a “flower-like” appearance.¹⁸

As the layers are brought closer together, the B cores from the two surfaces merge to form a single micelle that is situated halfway between the two surfaces (Figure 2b). The A chains from both surfaces now form a common shell around this central micelle. The merging of the micelles happens at a distance that is significantly greater than the vertical extent of the isolated micelles.^{8,10,12–14} As noted in the Introduction, this is due to the solvophobic interactions that drive the B cores to merge and thereby reduce the extent of polymer–solvent contact.

With further decreases in the surface separation, more solvent is expelled from the system and the density of the soluble component around the micellar core increases (Figure 2c). Note that the B cores now span the gap between the substrates.

In Figure 3, we plot the free energy of interaction, ΔF_{int} , as a function of surface separation, L . The interactions are repulsive when $\Delta F_{\text{int}} > 0$ and attractive when $\Delta F_{\text{int}} < 0$. ($\Delta F_{\text{int}} = 0$ when the surfaces are sufficiently far apart that the layers do not interact.) As the surfaces are initially brought together, the solvophilic A layers (or the “petals” of the flowers) come into contact and the free energy shows a minimal repulsion. When the B cores merge, the free energy of interaction begins to decrease (near $L = 18$). As the compression continues, however, there is a point at which the entropic losses start dominating and the free energy of interaction becomes repulsive.

If the chains are relatively incompatible, or $\chi_{AB} > 0$, the more soluble A chains are less able to shield the B component from the solvent. The extent of shielding is now determined by the competition between the enthalpic gain due to the reduction in B–solvent contacts and the enthalpic loss due to the energetically unfavorable A–B contacts. At $\chi_{AB} = 0.5$, there is still a tendency for the more soluble component to shield the solvent-incompatible B. If, however, χ_{AB} is increased to 1.5, the shielding behavior is significantly diminished. Figure 4 shows the conformation of the layers for a fixed surface separation of $L = 9$ with $\chi_{AB} = 1.5$. When the surfaces are far apart, the solvophilic A’s form a stretched brush. Compression of the surfaces again leads to the merging of the B micelles for the same reasons as for $\chi_{AB} = 0$. Now, however, the A chains do not encircle the B cores but, rather, spread out uniformly in the region between the two surfaces (compare Figures 4 and 2b).

The free energy of interaction as a function of surface separation for $\chi_{AB} = 0.5$ and 1.5 are also shown in Figure 3. The qualitative features in the cases of $\chi_{AB} > 0$ are similar to those for $\chi_{AB} = 0$, including the presence of an attractive region. The strength of attraction, however, decreases and the size of the attractive region shrinks as χ_{AB} increases. This is due to the extra enthalpic losses that arise from the A–B repulsion.

To illustrate how the interaction between the layers can be tailored by varying the relative chain lengths,¹⁰ we let the soluble A component be twice as long ($N_A = 80$) as the less soluble B component ($N_B = 40$). Since the area of the micellar core is smaller here than in the cases above (where $N_B = 80$), smaller

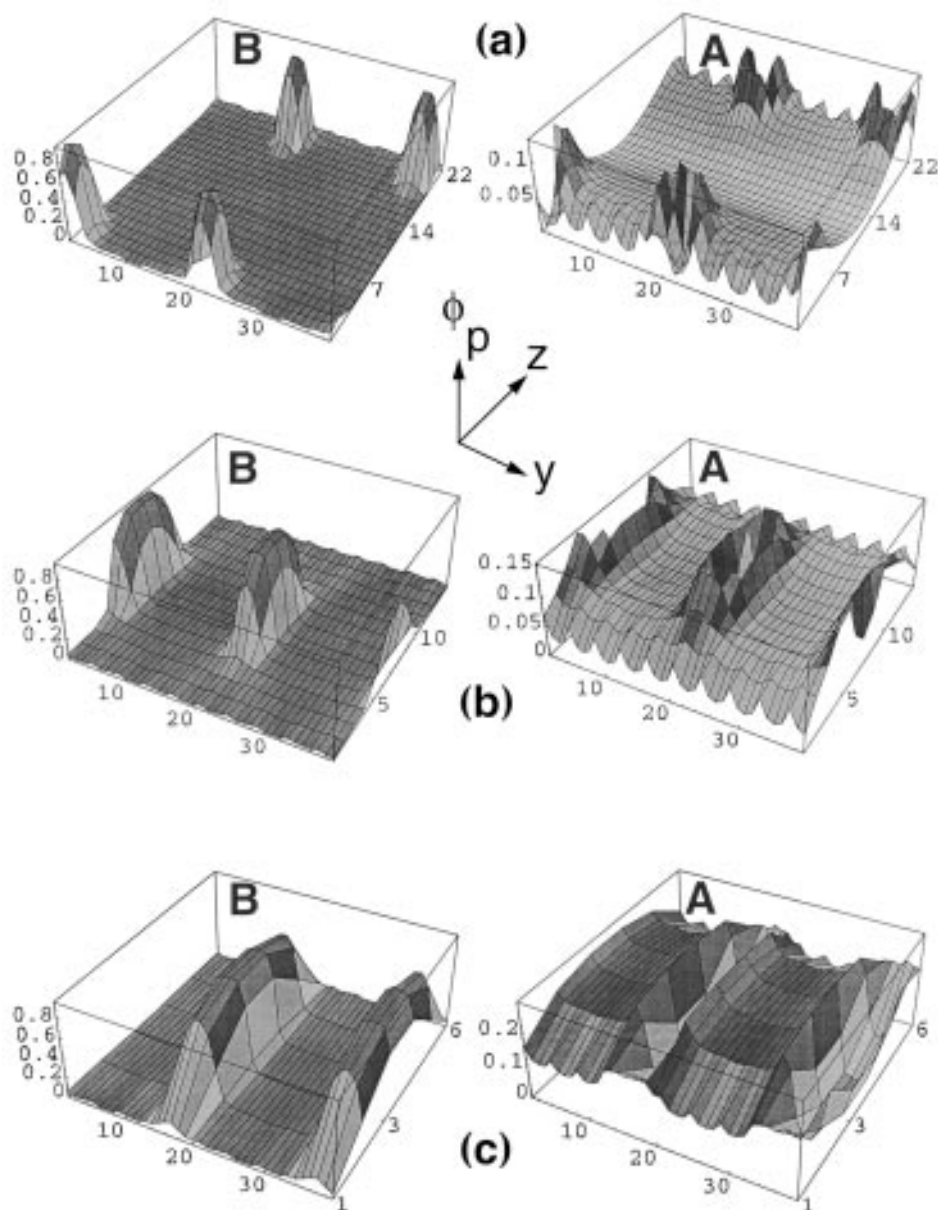


Figure 2. Three-dimensional plots showing the effect of decreasing the surface separation, L , for alternately grafted A–B chains where $N_A = N_B = 80$. Unless stated otherwise, the grafting density per line ρ is 0.025, $\chi_{AS} = 0$, $\chi_{BS} = 2$, and $\chi_{AB} = 0$ in all the subsequent figures. The figures are for the following surface separations: (a) $L = 21$, (b) $L = 13$, and (c) $L = 5$. The chains are grafted in the XY plane and ϕ_p denotes the polymer density. The plots marked “B” show the polymer density of the B blocks, while the plots marked “A” show the density of the A blocks.

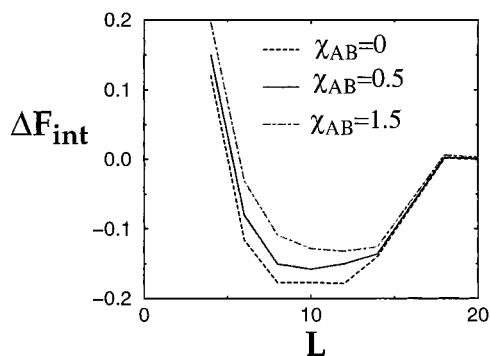


Figure 3. Free energy of interaction, ΔF_{int} , as a function of surface separation, L , for alternately grafted A–B chains where $N_A = N_B = 80$. The figure shows results for three different χ_{AB} , which are shown with different types of lines.

amounts of the A polymer are needed to shield the B domain and the rest of the soluble polymer forms a stretched layer. Now, as the surfaces are compressed, it is the longer A chains that

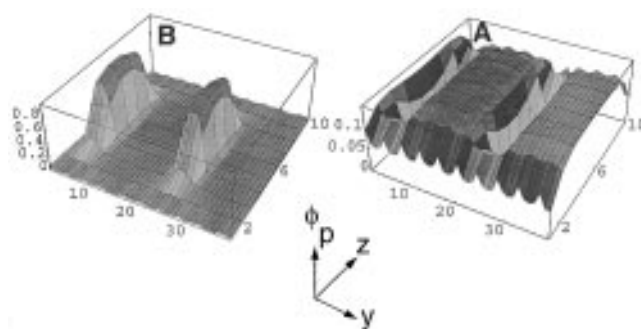


Figure 4. Three-dimensional plots showing the self-assembly for surface separation, $L = 9$, for alternately grafted A–B chains. Here, $\chi_{AB} = 1.5$.

initially come into close contact. The entropic losses associated with confining these solvophilic chains give rise to a repulsive interaction, as can be seen in the free energy of interaction in Figure 5. Further compression of the surfaces brings the micelles into contact and drives these cores to merge. The

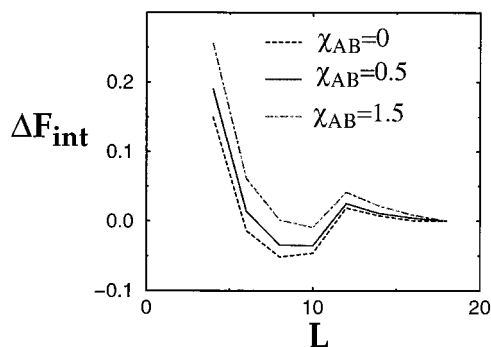


Figure 5. Free energy of interaction ΔF_{int} as a function of surface separation, L , for alternately grafted A–B chains with $N_A = 80$ and $N_B = 40$.

merger again give rises to an attraction between the plates. The lower volume fraction of the B component, however, shrinks the attractive region in the free energy of interaction.

Comparison of Figures 3 and 5 shows that the initial repulsion is more pronounced and the minima are higher in Figure 5. This behavior is consistent for all three values of χ_{AB} . These plots indicate that the overall shape of the curves can be controlled by manipulating the relative length of the different chains. We return to this point in our scaling analysis.

To highlight the advantages of having both A and B chains on *each* surface, we compare the above results to our findings on the system shown in Figure 1b.^{10,11} Here, one substrate is coated with $\chi_{AS} = 0$ chains, and the other is covered with $\chi_{BS} = 2$ homopolymers. The length of the chains is given by $N_A = N_B = 80$, and χ_{AB} is set at 0. As Figure 6 shows, there is an increase in the density of the soluble A component around the B micelles when the surfaces start interacting. Again, this behavior shields the solvophobic B's and thereby lowers the surface tension in the system. As the surfaces get closer, the morphology of the layers resembles the “flower-like” structure described above (see Figure 2a).

While the increased shielding of the B's leads to an enthalpic gain in the free energy, the surface confinement results in entropic losses. When $\chi_{AB} = 0$, the free energy of interaction plotted in Figure 7 displays a minute attractive region. When $\chi_{AB} > 0$, however, the surface interactions are purely repulsive. Absent from this system is the attraction that arises from the merging of micelles from opposite surfaces. The latter interactions can only occur by having solvophobic chains on *both* surfaces. Thus, the system where the A chains are localized on one surface and the B's on the other offers less “handles” or options for tailoring the surface interactions.

To further analyze and quantify the possible interactions between surfaces that contain both solvophilic A and solvophobic B homopolymers, we turn to scaling theory.^{10,19} The interaction potentials we calculate with this model can be classified into four distinct classes, as shown in Figure 8. In the first of these (Figure 8a), the interaction potential is *micelle-dominated*. This type of interaction is seen in Figure 3. Here, the interaction potential nearly vanishes for plate separations greater than $L = 18$. When the separation is lowered to $L = 18$, the effective attraction between the micelles drives the plates toward $L = 0$. When, however, the separation becomes too small, the soluble A chains are compressed, causing the eventual upturn in the interaction free energy for intermediate L . The second type of interaction (Figure 8d) is *brush-dominated*, which can be seen in Figure 7. The interaction potential is purely repulsive; the response of the system is dominated by the compression of the swollen A brush as the plates are brought together. The third type of interaction profile (Figure 8b)

resembles a *ratchet*. As in Figure 5, there is an initial repulsion between the surfaces, followed by a large attractive region and then further repulsion. If the surfaces are driven together with sufficient force to overcome the initial repulsion, they bind each other at the global minimum of the interaction. The fourth type of profile (Figure 8c) is hinted at in the upper curve in Figure 5, where $\chi_{AB} = 1.5$ and the minimum is barely attractive. With a slight increase in χ_{AB} , the global minimum near $L = 10$ becomes a local minimum. (The true global minimum of the interaction is at large plate separations.) In this case, there is a *metastable* equilibrium point in the free energy profile.

These interaction types (micelle-dominated, brush-dominated, ratcheting, and metastable) have different implications for controlling a solution of coated particles. Brush-dominated interactions stabilize the dispersion, while micelle-dominated interactions promote aggregation into clusters characterized by a well-defined, nonzero separation. Ratcheting interactions also promote aggregation with a well-defined separation. However, the initial repulsion has an effect on the kinetics of aggregation. A metastable interaction provides steric stabilization like that given in the brush-dominated regime. However, in thermodynamic equilibrium, there is a band of inaccessible particle separations near the kink in the free energy. We produce a properly concave interaction free energy by employing a Maxwell construction, as indicated by the dashed lines in Figure 8.

In our scaling model, each surface is again coated with A and B homopolymers, with an area per chain of s_A for the A chains and s_B for the B chains. The A chains have N_A monomers, and the B chains have N_B monomers. We assume that both the A and B chains are grafted relatively uniformly on each surface. We further assume that the solvent is good for A but poor for B. We define a solvent quality parameter $\tau = 2\chi - 1$, where $\chi > 1/2$ is the Flory–Huggins mixing parameter for B monomers and the solvent. We assume that $\chi_{AB} = \chi$, so that there is no shielding effect to consider. Finally, we assume that the respective monomer–surface interactions are given by $\chi_{AW} = 0$ and $\chi_{BW} = \chi$. Thus, the surface is nonadsorbing for both A and B.

At large separations, the B homopolymers form pinned micelles that coat the surfaces, and we assume that N_A and s_A are such that the A polymers form brushes. The situation is akin to that depicted in Figure 2a. (The important difference between the system pictured in Figure 2(a) and the one we consider here is that the A polymer does not shield the B cores.) We treat the A and B systems independently, as is justified in the absence of shielding and when the typical distance between adjacent micelles is large. We define H such that the plate separation, L , is given by $L = 2H$.

For simplicity, we employ the Alexander and de Gennes approximation for the A brush; that is, we assume that the free ends of the grafted chains are localized in a single plane parallel to the grafting surfaces.^{21,22} When the surfaces are far apart, the free energy per chain in the brush is given by

$$F(H) = \frac{3}{2} \frac{H^2}{a^2 N_A} + \frac{a^3 N_A^2}{H s_A} \quad (8)$$

where H is the as yet unknown height of the unperturbed brush and a^3 is the effective volume per monomer. Minimizing $F(H)$ with respect to H yields

$$H_{\text{br}} = 3^{-1/3} a^{5/3} s_A^{-1/3} N_A \quad (9)$$

and

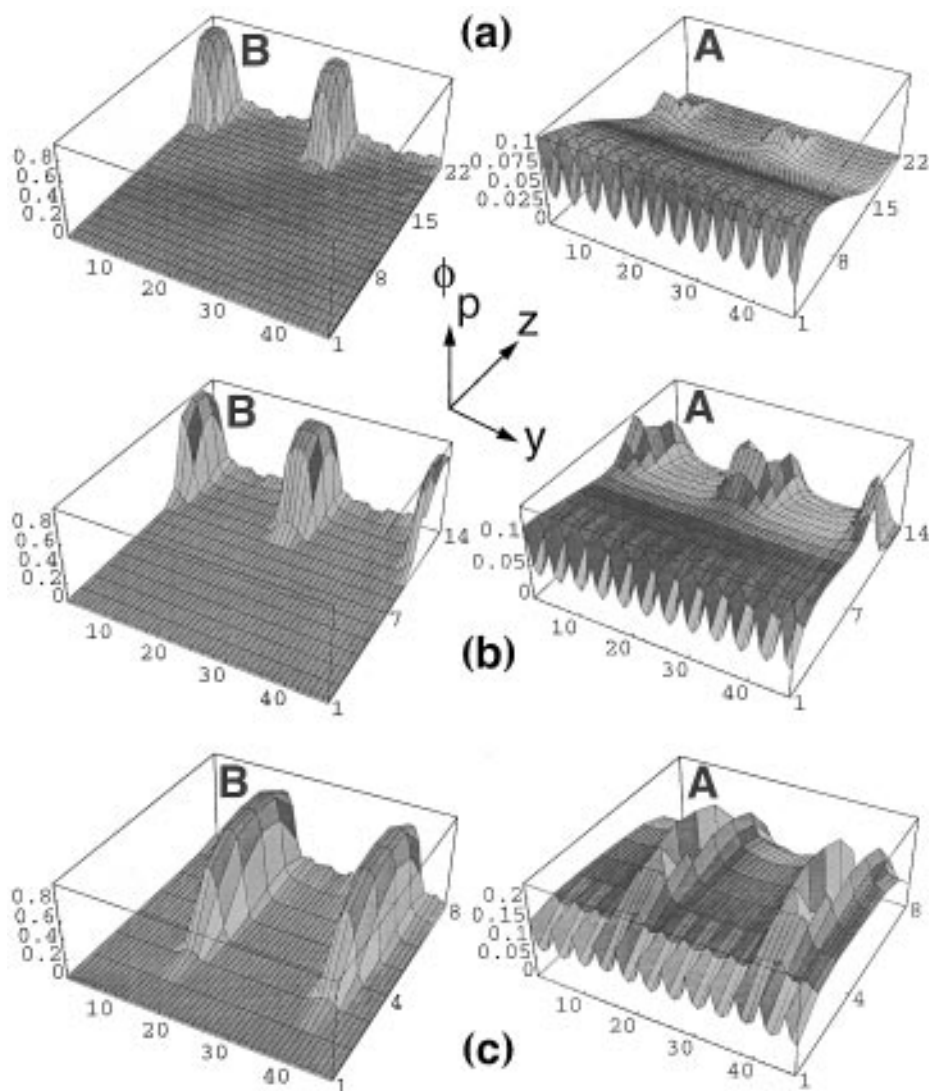


Figure 6. Three-dimensional plots showing the effect of decreasing the surface separation, L , when one surface is coated with A homopolymers and the other is coated with B chains. Plot are for (a) $L = 21$, (b) $L = 13$, and (c) $L = 7$. Here, $N_A = N_B = 80$ and $\chi_{AB} = 0$.

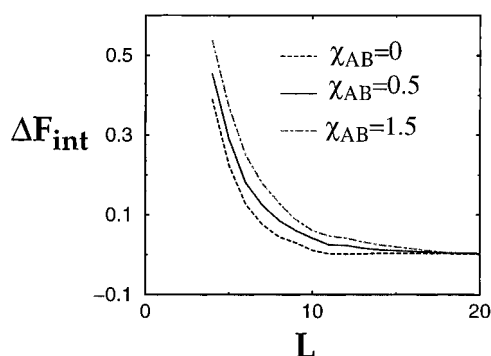


Figure 7. Free energy of interaction ΔF_{int} , as a function of surface separation, L , when one surface is coated with A homopolymers and the other is coated with B chains.

$$F_{\text{br}}^0 = (3^{4/3}/2)a^{4/3}s_A^{-2/3}N_A \quad (10)$$

where H_{br} is the undisturbed thickness of the brush and F_{br}^0 is the free energy per chain in the brush. Then, the interaction free energy of the brush per chain is

$$\Delta F_{\text{br}} = \begin{cases} 0 & \text{when } H \geq H_{\text{br}} \\ F_{\text{br}}^0 g\left(\frac{H}{H_{\text{br}}}\right) & \text{when } H \leq H_{\text{br}} \end{cases} \quad (11)$$

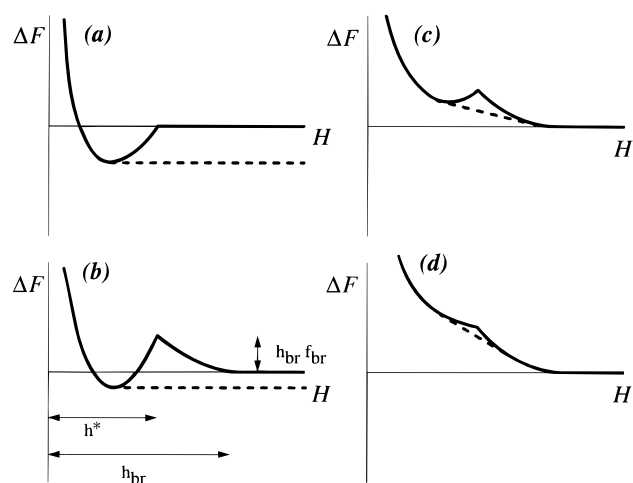


Figure 8. Interaction types. (A) Micelle dominated. The thermodynamic phases are $H = H_{\text{min}}$ and $H \rightarrow \infty$. The dotted line is produced by a Maxwell construction. (B) Ratchet. The thermodynamic phases are as in (A), but the adjustable repulsive tail has implications for the kinetics of aggregation. (C) Metastable. The interaction is generally repulsive, but near the local minimum there is a band (via the Maxwell construction) of unstable particle separations. (D) Brush dominated. There is no longer a local minimum in the interaction profile, and the unstable band is small.

where

$$g\left(\frac{H}{H_{\text{br}}}\right) = \frac{F(H/H_{\text{br}})}{F_{\text{br}}^0} - 1 = \frac{1}{3}\left(\frac{H}{H_{\text{br}}}\right)^2 + \frac{2}{3}\left(\frac{H_{\text{br}}}{H}\right) - 1 \quad (12)$$

Note that $g(1) = 0$; $F_{\text{br}}^0 g(x)$ is the difference in free energy between a compressed brush (with $x = H/H_{\text{br}} < 1$) and the uncompressed layer (where the brush thickness is equal to H_{br}). When $H > H_{\text{br}}$, the brushes are undisturbed, while if $H < H_{\text{br}}$, each brush is compressed at a cost in free energy.

The B system forms pinned micelles on each surface. At $H = H^*$, the B micelles merge to form micelles centered in the gap between the surfaces, with long stretched “legs” going from the micelle toward each surface. We first analyze the situation for separations with $H > H^*$, where the micelles are localized on the individual surfaces. The f chains in each micelle form a dense core, whose radius is $R = (fN_{\text{B}}/\tau)^{1/3}$, and legs that anchor the micellar core to the surface.⁵ The equilibrium characteristics of a pinned micelle containing f chains are determined by the balance of the surface free energy (per chain) of the core, ΔF_{surf} , and the free energy associated with the elastic stretching of a leg, ΔF_{leg} . The ΔF_{surf} term arises from the surface tension (which is proportional to τ^2) at the boundary between the core and the solvent and is given by $\Delta F_{\text{surf}} = 4\pi\tau^2 R^2/f$. Since the lateral size of the micelles is $D = (fs_{\text{B}})^{1/2}$, then $\Delta F_{\text{leg}} = \tau D = \tau(fs_{\text{B}})^{1/2}$. (Here, $D \gg R$.) Minimizing the sum of $\Delta F_{\text{surf}} + \Delta F_{\text{leg}}$ with respect to R yields the equilibrium dimensions of a pinned micelle⁵

$$D_{\text{pm}} = \left(\frac{2}{3}\right)^{3/5} \pi^{-1/5} a^{3/5} \tau^{1/5} s_{\text{B}}^{1/5} N_{\text{B}}^{2/5} \quad (13)$$

and gives

$$F_{\text{pm}} = 5(108\pi)^{-1/5} a^{-2/5} \tau^{6/5} s_{\text{B}}^{1/5} N_{\text{B}}^{2/5} \quad (14)$$

where D_{pm} is the lateral extent of the equilibrium structure and F_{pm} is the free energy per chain in the pinned micelle state.

The pinned micelle will also form in the gap between the surfaces. Then, the free energy per chain has the form¹³

$$F = 4\pi\tau^2 R^2/2f + (D^2 + H^2)^{1/2} \tau \quad (15)$$

The surface energy per chain is lowered by a factor of 2, since the common micelle is made of $2f$ chains, f coming from each surface. Following the calculation outlined above, and expanding eq 15 for small H (with the understanding that $R \ll H$) the H -dependent free energy of the centered micelle is

$$F_{\text{c}} = F_{\text{pm}} \left(2^{-1/5} + \frac{2^{1/5}}{5} \frac{H^2}{D_{\text{pm}}^2} \right) + O\left[\frac{H}{D_{\text{pm}}}\right]^3 \quad (16)$$

(Note, the notation $O[x]$ means “on the order of x .”) For $H \ll D_{\text{pm}}$, the free energy per chain is lower than the state where the micelles are formed separately on the walls, but the free energy rises as the stretching is increased by an increase of H . Eventually, the centered micelles divide into two and jump to each surface, at which point the free energy per chain becomes constant in H . The transition occurs near $H/D_{\text{pm}} \approx O[1]$. The transition point may be analyzed by expanding eq 15 about $D = D_{\text{pm}}$ and $H = D_{\text{pm}}$ to second order. From this expansion, we find that the jumping transition occurs at $H^* = 0.823D_{\text{pm}}$. We approximate $F_{\text{c}}(H)$ for $H < H^*$ by a quintic polynomial that matches the expansions for small H and for H near D_{pm} .^{10,19}

We now define $\Delta F_{\text{c}} = F_{\text{c}}(H) - F_{\text{pm}}$. The total interaction free energy, ΔF , is defined by

$$\Delta F = \Delta F_{\text{br}} + \Delta F_{\text{c}} \quad (17)$$

$\Delta F(H)$ differs from ΔF_{int} above in that ΔF is a free energy per chain, while ΔF_{int} is loosely the free energy per unit area. ΔF can be classified into one of the above four categories, as demonstrated in Figure 9. We define two parameters: $f_{\text{br}} = F_{\text{br}}/F_{\text{pm}}$, and $h_{\text{br}} = H_{\text{br}}/D_{\text{pm}}$. When $h_{\text{br}} < h^* = 0.823$, the potential is micelle-dominated. This corresponds to region A. The micelles merge before the brushes come into contact, so that there is always an attractive region (not preceded by an initial repulsion). When $h_{\text{br}} > h^*$, the behavior of the potential is controlled by f_{br} . For large f_{br} , the potential is purely repulsive, but there is a kink in the free energy near $H = H^*$. This is region D. As f_{br} is decreased, a local minimum appears in the potential (region C), and if f_{br} is decreased even further, this local minimum becomes the true global minimum (region B). The boundary between regions D and C and the boundary between regions B and C are asymptotically of the form $f_{\text{br}} \sim h_{\text{br}}^{-1}$ in the limit $h_{\text{br}} \gg 1$.

Since adjusting N_{A} and s_{A} provides independent control over f_{br} and h_{br} , by tailoring N_{A} and s_{A} we may in principle choose the interaction type from among the above four. Additionally, when the interaction is of the ratcheting type (Figures 8b and 9), control over the range and free energy barrier of the interaction can be gained by correctly designing the coverage and molecular weight of the soluble component. This fine level of control should be relatively easy to achieve experimentally and low in cost to implement and is of significant utility in designing tunable colloidal dispersions for specific applications.

We note that effects similar to those observed with the two distinct homopolymers can be achieved by grafting copolymers that contain both solvophilic and solvophobic blocks.^{12,13} Consider the case where each surface is coated with symmetric AB diblocks, which are grafted by the ends of the B blocks, and $\chi_{\text{AS}} = 0$, $\chi_{\text{BS}} = 2$, and $\chi_{\text{AB}} = 0$. When the layers are far apart, these chains also form “flower”-like structures on each of the surfaces.¹⁸ In particular, the solvophobic B blocks form a dense core and the A chains form a broad corona around this B region. As a consequence, the interaction profiles are similar to those in Figure 3. Modifications in the surface interactions can be achieved by varying χ_{AB} , the relative lengths of the solvophilic and solvophobic components, or tethering the chains by the end of the A blocks.¹² Thus, tethered copolymers also provide a means of engineering the interactions between the substrates.

Interactions between Like-Charged Polymer Layers. An additional way of controlling the surface interactions is to anchor polyelectrolytes on the substrates. The behavior of this system is rather complex in a poor solvent.^{14,23} While the incompatibility with the surrounding solvent drives the chains to collapse into pinned micelles, the electrostatic interactions give rise to a repulsion, which favors the disruption of the micelles. The final structure will depend on a balance between these competing interactions and will clearly depend on the degree of the polymer–solvent incompatibility and the extent to which the chains are charged. We first determine the structure of the layer on one surface²³ and then investigate how this structure affects the interaction between two surfaces.¹⁴ In our single-surface study, we begin our analysis by deriving the scaling behavior for the charged pinned micelles and use 2D SCF¹⁶ calculations to visualize these structures. (In the latter SCF model for charged polymers, there is an additional contribution to the potential that arises from the electrostatic interactions between different charged species.¹⁶)

We consider flexible homopolymers that are anchored by one end onto an inert, planar substrate. The chains are grafted at

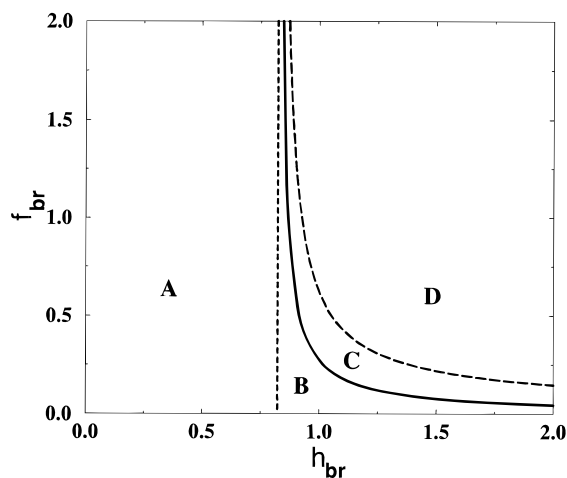


Figure 9. Diagram of interaction types. (A) Micelle-dominated interactions. The coalescence of the micelles dominates the free energy of interaction. There is a single global minimum and no initial repulsion in the interaction free energy. (B) Ratcheting interactions. The interaction free energy has an initial repulsion that shields the global minimum. (C) Metastable interactions. There is a cusp in the free energy, followed by a local minimum. The free energy is repulsive and provides steric stabilization. (D) Brush dominated. The free energy is purely repulsive, although there is a cusp in the interaction when the micelles merge.

relatively low densities, and the system is immersed in a poor solvent. The area per chain²⁴ is given by the parameter s and each chain contains $N \gg 1$ segments. The degree of ionization per chains is specified by α . This is, each chain has $q = \alpha N$ immobilized charges and produces an equal number of q mobile counterions in the solution, which is assumed to be salt-free. We also assume that the Bijerrum length $l_B = e^2/\epsilon kT = a$, which is typical for flexible, water soluble polymers. Here, e is the unit of elementary charge, ϵ is the dielectric constant of the solvent, and a is the diameter of a monomer.

As noted above, the equilibrium characteristics of a neutral ($\alpha = 0$) pinned micelle are determined by the balance of the surface free energy (per chain) of the core, ΔF_{surf} , and the free energy associated with the elastic stretching of a leg, ΔF_{leg} . Minimizing the sum of $\Delta F_{\text{surf}} + \Delta F_{\text{leg}}$ with respect to f yields the equilibrium dimensions of the neutral pinned micelle (neglecting all numerical coefficients):⁵

$$f_o = N^{4/5} \tau^{2/5} / s^{3/5}; \quad R_o = N^{3/5} / (\tau^{1/5} s^{1/5}); \quad D_o = N^{2/5} \tau^{1/5} s^{1/5} \quad (18)$$

The presence of charged groups within the chains leads to an additional free energy contribution, ΔF_{elec} , which arises from the electrostatic interactions between charges and the translational entropy of the mobile counterions. When α is small, the attraction between the charged core and the mobile counterions is insufficient to localize the ions in the vicinity of micelles; thus, the micelles are weakly charged. An increase in α leads to the localization of the ions near the cores and a partial screening of the Coulomb repulsion. The onset of counterion condensation occurs at $\alpha = \alpha_o$, the point at which the net charge of the core, $Q = \alpha f N$, equals the radius of the core,²⁵ R , or $Q = R$. At $\alpha \gg \alpha_o$, the majority of the counterions are trapped inside the cores and only a small fraction of the counterions, $\approx R/Q$, are still found outside the micelles.

For significantly poor solvents, or $0 < \tau \leq 1$, the charged micelles are still described by the scaling dependences in eq 18.²³ Thus, $\alpha_o = R_o/f_o N = s^{2/5} N^{-6/5} \tau^{-3/5}$, which is significantly less than 1. Consequently, the condensation threshold is quite

low, and the counterions are primarily localized within the pinned micelles.

The trapped counterions give rise to a contribution $\Delta F = N\alpha \ln(\alpha\tau)$ and create an osmotic pressure that partially swells the core. Eventually, the osmotic pressure produced by these trapped counterions disrupts the micelles and transforms the patterned layer into a laterally homogeneous swollen brush, which has a thickness^{25,26} $H = N\alpha^{1/2}$. The point at which this transition occurs, α^* , is determined by equating the chemical potentials of the chains in a micelle, μ_c , and in a homogeneous layer, μ_s . In a micelle, the major contributions to μ_c arise from the polymer–polymer attractions and the translational entropy of the trapped counterions, yielding $\mu_c = -N\tau^2 + \alpha N \ln(\alpha\tau)$. In a swollen layer, μ_s is determined by the elastic stretching of the chains and the translational entropy of the mobile counterions, yielding $\mu_s = H^2/N + \alpha N \ln(\alpha N/sH)$. Substituting $H = N\alpha^{1/2}$ into the expression for μ_s and equating μ_c and μ_s , we obtain²⁷ (neglecting logarithmic prefactors) $\alpha^* = \tau^2$ and thus, the height of the layer at α^* is $H^* = N\tau$.

To visualize the changes that occur within the tethered layer as α is increased, we turn to the 2D SCF calculations.^{14,23} Here, $s = 100$, the length of the chains is fixed at $N = 100$, and χ , the polymer–solvent interaction parameter, equals 2. (This χ value corresponds to $\tau \approx 1$ in our scaling model, and here, $\alpha_o \approx 0.01$.) Figure 10 reveals the equilibrium profiles of the polymer and mobile ions at various α values for the single surface case. At $\alpha = 0$ (neutral chains), the polymers form well-defined pinned micelles with dense cores (ϕ , the polymer density, ≈ 0.9). At $\alpha = 0.15$, the counterions have predominantly condensed into and partially swollen the cores. (The volume fraction of polymer in the cores diminishes, and the total size of the micelle increases slightly.) At $\alpha = 0.27$, the micelles have been destroyed, and the laterally homogeneous layer is swollen by counterions. For these values of the parameters, the transition point from pinned micelles to a uniform brush occurs at $\alpha^* = 0.23$.

We expect that the interaction between two such polyelectrolyte-coated surfaces is different for the $\alpha < \alpha^*$ and $\alpha > \alpha^*$ regimes.¹⁴ At $\alpha < \alpha^*$, the surfaces are covered with pinned micelles at all surface separations h . Since the counterions are predominantly condensed within the micelles, the initial repulsion between the surfaces due to noncondensed counterions is rather weak. As in the case of neutral polymers, when the layers are brought into contact, micelles from the opposite surfaces merge at $h = D_o$, and this merger gives rise to an attractive minimum.

The situation is qualitatively different at $\alpha > \alpha^*$. Here, the surfaces are covered by swollen brushes at infinite plate separations. As these surfaces are compressed, the counterions undergo significant losses in translational entropy. At a critical deformation h^* , the attractive polymer–polymer interactions will override the entropic contributions and the homogeneous, dilute layers abruptly transform into collapsed, pinned micelles. This structural transformation constitutes a first-order phase transition and is accompanied by a significant redistribution of all the components. When the layers are compressed further, so that $h < h^*$, micelles from the opposite surfaces again merge at $h = D_o$.

The different morphologies between the two surface for $\alpha > \alpha^*$ can be seen from the density profiles obtained through the SCF calculations. The profiles in Figure 11a reveal the laterally homogeneous layer at large separations, or $h > h^*$; Figure 11b shows the appearance of distinct pinned micelles on each surface when $h = h^*$. The merging of the micelles into larger structures between the plates can be seen in Figure 11c, where $h < h^*$.

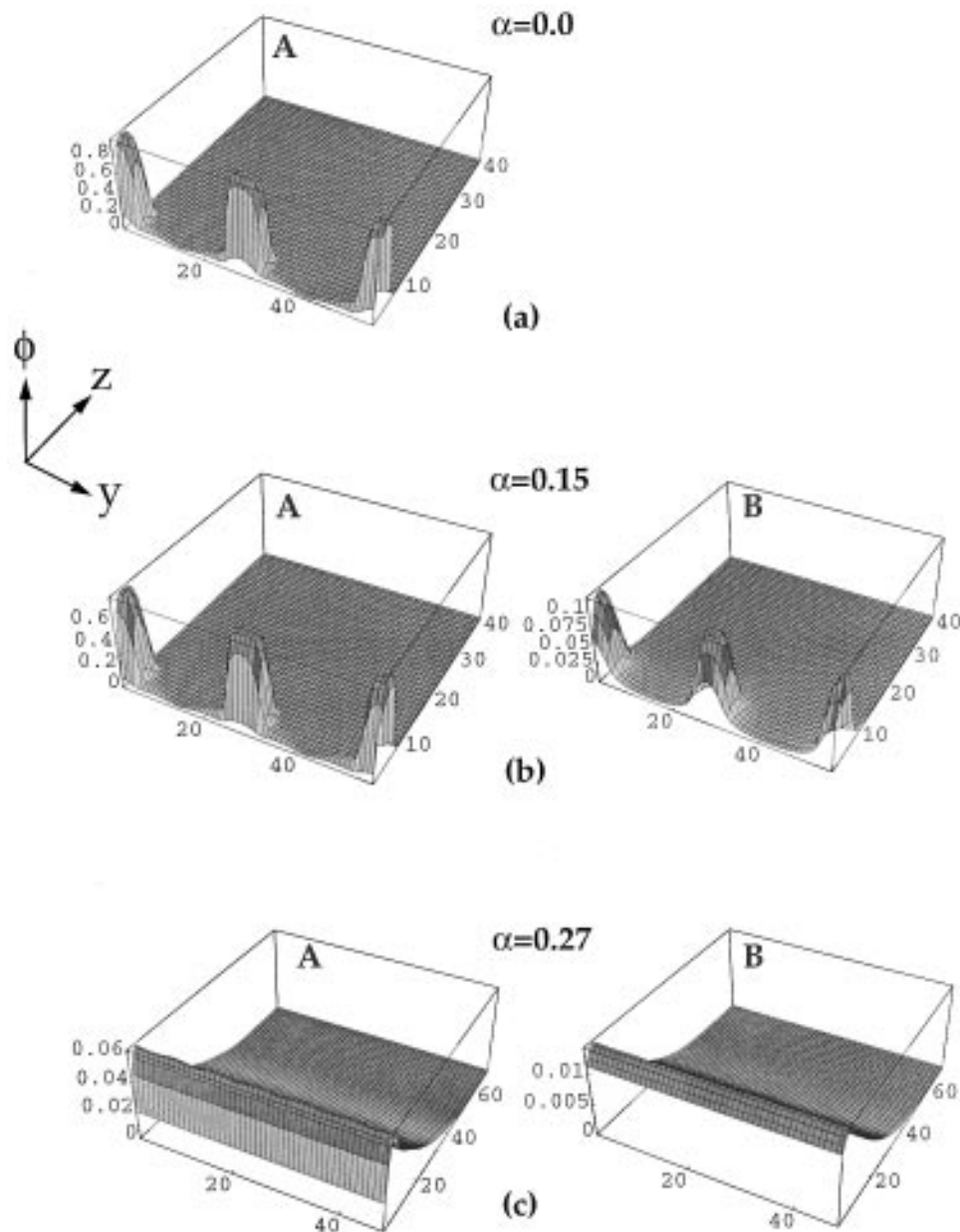


Figure 10. Three-dimensional SCF density profiles for the polymer and counterions showing the effect of increasing the degree of ionization, α , for $N = 100$, $s = 100$, and $\chi = 2$. The chains are grafted in the XY plane, the Z direction lies perpendicular to the surface, and ϕ denotes the polymer (A) or counterion (B) density. In (a), $\alpha = 0.0$, (b) $\alpha = 0.15$, and (c) $\alpha = 0.27$.

We can determine the specific value of h^* by equating the chemical potentials of the chains in the stretched layers, μ_s , and that in the collapsed micelles, μ_c . Introducing the reduced variable $\beta = h^*/H^*$ (where H^* is the height of the swollen brush at $\alpha = \alpha^*$), we can write $h^*(\alpha)$ in the following form

$$\alpha/\alpha^* = [\gamma - (1 - \beta^2)/2]/[\gamma + \ln(\beta)] \quad (19)$$

where $\gamma = \ln(\tau^2 s) > 1$ and all the necessary prefactors have been retained. Through eq 19, we can delineate the phase boundary between the two states of the system, pinned micelles versus a homogeneous layer, for both undeformed ($\beta = 1$) and compressed ($\beta < 1$) layers. This expression indicates that β is a decreasing function of α ; i.e., a greater compression is necessary to cause the formation of pinned micelles at higher values of α . To illustrate this behavior, Figure 12 shows a plot of h^* versus α , which was obtained from the SCF calculations. Above the solid line, the system forms a laterally homogeneous layer, while below this line, the chains collapse into pinned micelles. As can be seen, this curve is in agreement with the

scaling prediction that h^* , the critical separation where the micelles appear, is a decreasing function of α .

To quantify the interaction between the surfaces, we use the SCF model to calculate the interaction free energy, ΔF_{int} , as the two surfaces are brought into contact for various values of α . This curve is shown in Figure 13. For small α 's ($\alpha < \alpha^*$), there is an initial increase in ΔF_{int} , which is caused by the osmotic pressure of the noncondensed counterions; this is followed by a pronounced attractive minimum that arises from the merging of micelles from opposite surfaces. An increase in α leads to a corresponding increase in the osmotic pressure of the noncondensed part of the counterions and a decrease in the attractive minimum. However, a nonmonotonic dependence of ΔF_{int} on h is still evident at rather high values of $\alpha \gg \alpha^*$, where each layer forms a laterally homogeneous, swollen brush. The nonmonotonic behavior is due to the novel effect noted above: the compression of these swollen brushes leads to the formation of pinned micelles at both surfaces. In Figure 13, the point at which this transformation occurs, or h^* , is pinpointed

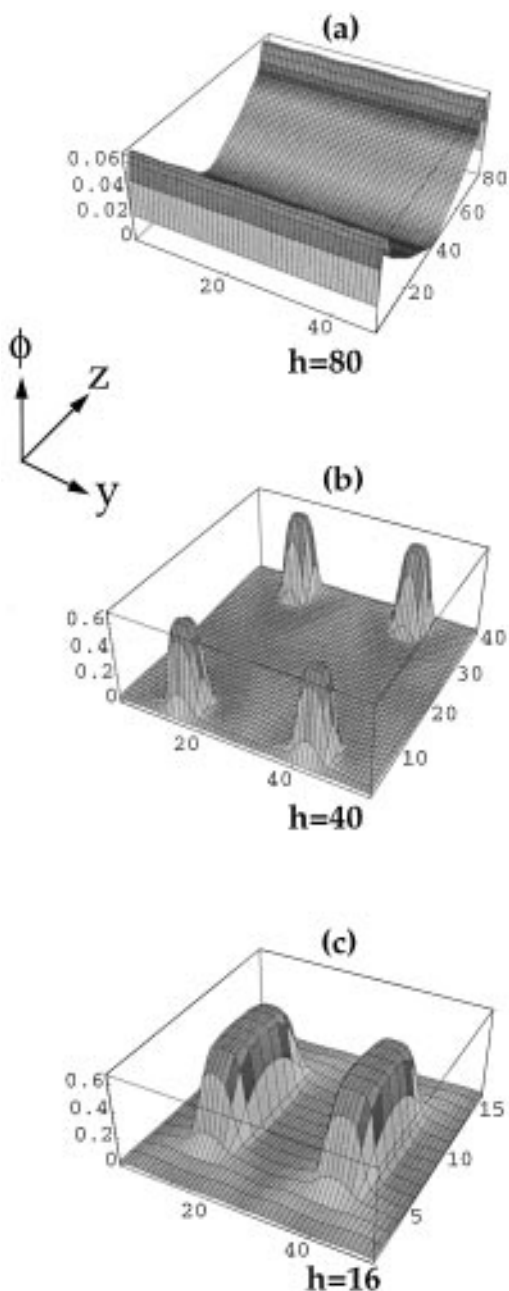


Figure 11. Three-dimensional SCF plots showing the effect of decreasing the surface separation for $N = 100$, $s = 100$, $\chi = 2$, and $\alpha = 0.27$. The chains are grafted in the XY plane, the Z direction lies perpendicular to the substrate, and ϕ denotes the polymer density. Here, the shape of the profiles for the counterions are qualitatively the same as those for the polymers. (a) At surface separation $h = 80$, the grafted chains form homogeneous layers. (b) At $h = 40$, micelles form on each of the surfaces. (c) At $h = 16$, compression causes the micelles from the surfaces to merge.

by a vertical arrow. (In these SCF calculations, the changes in free energy as a function of h are so small that a discontinuity in the slope, which characterizes this first-order transition, is not evident in the figure.) Below this surface separation, the curves display a distinct minima, which once more arises from the association of the micelles from the opposite surfaces (as shown in Figure 11c). Note, however, that this minima finally disappears for higher values of α .

The specific positions of the various minima are not affected by the value of α (see Figure 13). For both $\alpha > \alpha^*$ and $\alpha < \alpha^*$ the location of the minimum is determined by the lateral periodicity of the system, D , since the merging of the micelles

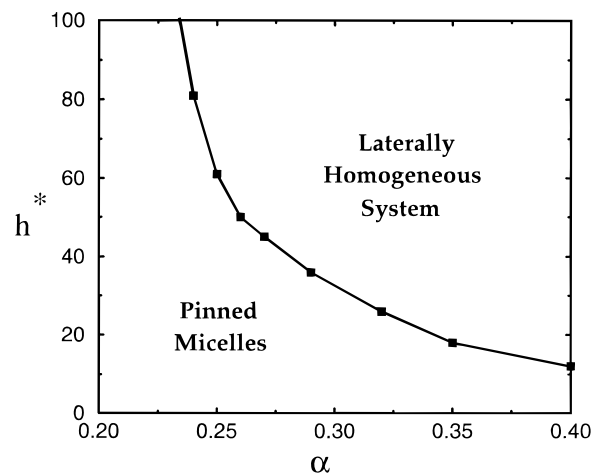


Figure 12. Phase boundary for the first-order phase transition separating the homogeneous layers from the inhomogeneous layer of pinned micelles. For a fixed α and $h < h^*$, the inhomogeneous system is favored over the homogeneous layer.

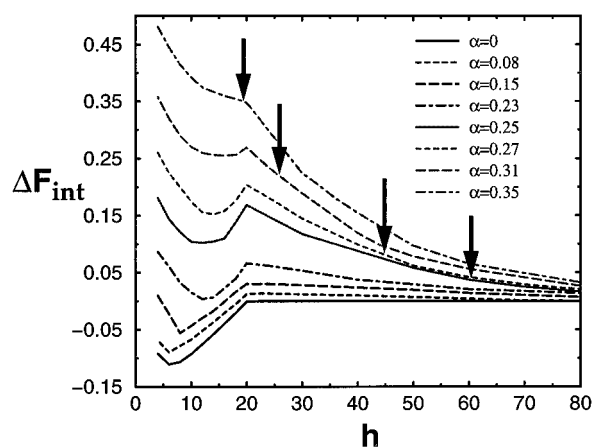


Figure 13. Free energy of interaction as a function of surface separation for $N = 100$, $s = 100$, $\chi = 2$, and values of α ranging from 0 (no charge) to 0.35 (approximately one charge per three monomers). The arrows in the plot pinpoint the transition from a homogeneous layer to pinned micelles.

occurs at $h \approx D$. For the values of the parameters examined here, D is not affected by α and, within reasonable accuracy, equals D_0 . (This can be seen, for example, by comparing the lateral extent of the micelles in Figure 10a, where $\alpha = 0$, and Figure 10b, where $\alpha = 0.15$.)

The appearance of the minima in Figure 13 has important practical implications. Our results are applicable to a system of polyelectrolyte-coated colloidal particles; this system will exhibit a similar free energy profile. The relatively sharp minima indicate that there is an optimal separation between the coated particles, and thus, these colloids could form an ordered array. (While the minimum for $\Delta F_{\text{int}} > 0$ represent metastable states, they are nonetheless experimentally accessible and may be long-lived.) Thus, our results indicate that by increasing the concentration of these colloids in solution, and thus effectively decreasing the surface separation h , the system can be driven into an ordered state. Such crystals can be used as tunable diffraction gratings or optical switching devices.^{28,29} Given the potential that these materials hold for fabricating novel optoelectronic devices, it is of significant technological importance to establish effective pathways for creating such ordered colloidal arrays.

Conclusions

We calculated the interaction between surfaces that are coated with a binary mixture of A and B homopolymers. The B polymers are in a poor solvent. We found that the free energy of interaction has a large attractive region even though the A component is in a good solvent. This behavior is observed even when the solvophilic component is twice as long as the solvophobic chains and, thus, makes the first contact with the opposing surface. The attraction between the surfaces is due to the formation of novel self-assembled structures as the surfaces are brought into contact. Note that the formation of pinned micelles, and the self-assembly between the layers, only occurs at low grafting densities. Thus, the behavior observed in these studies is in sharp contrast to the behavior of the system at high grafting densities, where the chains form dense brushes and 1D SCF calculations indicate the surfaces exhibit a monotonic repulsion.⁹

These findings provide guidelines for controlling the interactions between polymer-coated substrates in solution. The results reveal that specified interactions can be obtained by grafting a low volume fraction of solvophobic and solvophilic chains and tailoring the A–B energies, the relative lengths, and coverages of the different homopolymers.

Our analysis on the tethered polyelectrolytes yield further prescriptions for tailoring the surface interactions. In particular, our findings indicate that the position of the minimum is governed by the lateral periodicity of the system, D_o , (i.e., by the parameters N and s), while the depth is predominantly affected by the value of α . One means of manipulating α is to vary the ionic strength of the solution. Thus, by varying the ionic strength, one can effectively decrease the strength of the electrostatic interactions and additionally tailor the interactions between the particles.

The above calculations also suggest an important direction for future research. During the preparation and processing of colloidal suspensions, a number of cosolvents are commonly added to the solution. The presence of multiple fluid components will even affect the conformation of a single-component grafted layer. Consider, for example, a layer of A homopolymers immersed in a mixed solvent. The behavior of this system is relatively complicated.^{30–33} Now, the height of the layer depends not only on the polymer–solvent interactions but also on the mutual compatibility of the solvents. In particular, a brush can collapse in a mixture of two good solvents, if these liquids are relatively more compatible with each other than they are with the polymer.³³ In the opposite limit, where the two solvents have a greater affinity for the polymer than for each other, the brush can swell, even in a mixture of two poor solvents.³³ When the mixed solvents are highly immiscible, the mixture will undergo a phase separation. If the amount of one component is relatively low, the mixture will phase separate inside a polymer brush and the demixing of the solvents could be exploited to control the brush height. In particular, for a polyacid brush (where the charge on layer depends on the local pH), the height can be significantly increased by adding a small amount of water to the oil solvent.^{34,35} This result suggests that the addition of the water can promote the stabilization of polymer-coated colloids in oil. SCF or other theoretical calculations on interactions between polyacid-coated surfaces in oil/water mixtures would clarify the behavior of such systems and could provide guidelines for fabricating new polymeric stabilizers.

Acknowledgment. A.C.B. and E.Z. gratefully acknowledge support from the NSF, through Grant DMR-9709101. A.C.B. and C.S. gratefully acknowledge support from the DOE, through Grant DE-FG02-90ER45438. A.C.B. and G.P. gratefully acknowledge support from ONR through Grant N00014-91-J-1363

References and Notes

- (1) Napper, D. H. *Polymer Stabilization of Colloidal Dispersion*; Academic Press: London, 1983.
- (2) Halperin, A.; Tirrell, M.; Lodge, T. P. *Adv. Polym. Sci.* **1991**, *31*, 100.
- (3) (a) Klein, J.; Kamiyama, Y.; Yoshizawa, H.; Israelachvili, J. H.; Fredrickson, G. H.; Pincus, P.; Fetters, L. J. *Macromolecules* **1993**, *26*, 5552. (b) Klein, J.; Perahia, D.; Warburg, S. *Nature* **1991**, *352*, 143. (c) Taunton, J.; Toprakcioglu, C.; Fetters, L. J.; Klein, J. *Nature* **1988**, *332*, 712. (d) Taunton, J.; Toprakcioglu, C.; Fetters, L. J.; Klein, J. *Macromolecules* **1990**, *23*, 571. (e) Hadziannou, G.; Patel, S.; Granick, S.; Tirrell, M. *J. Am. Chem. Soc.* **1986**, *108*, 2869. (f) Patel, S.; Tirrell, M. *Annu. Rev. Phys. Chem.* **1989**, *40*, 597. (g) Israelachvili, J. N.; Tandon, R. K.; White, L. R. *Nature* **1977**, *277*, 120.
- (4) The height of the brush now scales as H/τ , where τ measures the deviation from the θ -temperature and is >0 .
- (5) (a) Klushin, L. I. unpublished work. (b) Williams, D. R. M. *J. Phys. II* **1993**, *3*, 1313. (c) Zhulina, E. B.; Birshtein, T. M.; Priamitsyn, V. A.; Klushin, L. I. *Macromolecules* **1995**, *28*, 8612.
- (6) (a) Lai, P.; Binder, K. *J. Chem. Phys.* **1992**, *97*, 586. (b) Yeung, C.; Balazs, A. C.; Jasnow, D. *Macromolecules* **1993**, *26*, 1914. (c) Huang, K.; Balazs, A. C. *Macromolecules* **1993**, *26*, 4736. (d) Grest, G. S.; Murat, M. *Macromolecules* **1993**, *26*, 3108. (e) Soga, K. G.; Guo, H.; Zuckermann, M. J. *Europhys. Lett.* **1995**, *29*, 531.
- (7) (a) Siqueira, D. F.; Kohler, K.; Stamm, M. *Langmuir* **1995**, *11*, 3092. (b) Zhao, W.; Krausch, G.; Rafailovich, M.; Sokolov, J. *Macromolecules* **1994**, *27*, 2933. (c) O'Shea, S. J.; Welland, M. E.; Rayment, T. *Langmuir* **1993**, *9*, 1826. (d) Stamouli, A.; Pelletier, E.; Koutsos, V.; van der Vegte, E.; Hadziannou, G. *Langmuir* **1996**, *12*, 3221.
- (8) Singh, C.; Balazs, A. C. *J. Chem. Phys.* **1996**, *105*, 706.
- (9) Chen, C.; Dan, N.; Dhoot, S.; Tirrell, M.; Mays, J.; Watanabe, W. *Isr. J. Chem.* **1995**, *35*, 41.
- (10) Singh, C.; Pickett, G.; Balazs, A. C. *Macromolecules* **1996**, *29*, 7559.
- (11) Balazs, A. C.; Singh, C. In *Morphological Control of Polymer Mixtures*; Briber, R., Peiffer, D., Eds., Materials Research Society: Pittsburgh, PA 1997; Vol. 461, p 115.
- (12) Singh, C.; Balazs, A. C. *Macromolecules* **1996**, *29*, 8904.
- (13) Balazs, A. C.; Singh, C.; Zhulina, E.; Gersappe, D.; Pickett, G. *Mater. Res. Soc. Bull.* **1997**, *22*, 16.
- (14) Singh, C.; Zhulina, E.; Balazs, A. C. *Macromolecules* **1997**, *30*, 7004.
- (15) (a) Huang, K.; Balazs, A. C. *Phys. Rev. Lett.* **1991**, *66*, 620. (b) Huang, K.; Balazs, A. C. *Macromolecules* **1993**, *26*, 4736.
- (16) Israels, R.; Gersappe, D.; Fasolka, M.; Roberts, V. A.; Balazs, A. C. *Macromolecules* **1994**, *27*, 6679.
- (17) Fleer, G.; Cohen-Stuart, M. A.; Scheutjens, J. M. H. M.; Cosgrove, T. Vincent, B. *Polymers at Interfaces*; Chapman and Hall: London, 1993.
- (18) Zhulina, E.; Singh, C.; Balazs, A. C. *Macromolecules* **1996**, *29*, 8254.
- (19) Pickett, G.; Balazs, A. C. *Macromol. Symp.* **1997**, *121*, 269.
- (20) If the A and B chains are grafted randomly on each surface, the results are the same as those for the alternately grafted case as long as the random distribution of chains is relatively uniform.
- (21) Alexander, S. J. *Phys. (Paris)* **1977**, *38*, 983.
- (22) de Gennes, P.-G. *J. Phys. (Paris)* **1976**, *37*, 1443.
- (23) Zhulina, E.; Singh, C.; Balazs, A. C., *J. Chem. Phys.*, in press.
- (24) As shown in ref 5a, for stable pinned micelles, $s_1 < s < s_2$, where $s_2 = N^{4/3}\tau^{2/3}$ and $s_1 = N^{1/2}/\tau$.
- (25) Pincus, P. A. *Macromolecules* **1991**, *24*, 2919.
- (26) Borisov, O. V.; Birshtein, T. M.; Zhulina, E. B. *J. Phys. II* **1991**, *I*, 521.
- (27) The same scaling dependence applies to the collapsed-to-stretched transition in laterally homogeneous charged brushes; see ref 26.
- (28) See, for example: Asher, S. A.; et al. *Science* **1996**, *274*, 959 and references therein.
- (29) (a) Larsen, A. E.; Grier, D. G. *Nature* **1997**, *385*, 230. (b) Larsen, A. E.; Grier, D. G. *Phys. Rev. Lett.* **1996**, *76*, 20.
- (30) Auroy, P.; Auvray, L. *Macromolecules* **1992**, *25*, 4134.
- (31) Marko, J. F. *Macromolecules* **1993**, *26*, 313.
- (32) Lai, P.-Y.; Halperin, A. *Macromolecules* **1992**, *25*, 6693.
- (33) Birshtein, T. M.; Lyatskaya, Y. V. *Macromolecules* **1994**, *27*, 1256.
- (34) de Gennes, P. G. *C. R. Acad. Sci., Ser. IIb* **1996**, *322*, 819.
- (35) Lyatskaya, Y.; Balazs, A. C. *Macromolecules*, in press.